Hindawi Publishing Corporation
Advances in Meteorology
Volume 2013, Article ID 170387, 11 pages
http://dx.doi.org/10.1155/2013/170387

Research Article

Trends and Variability of North Pacific Polar Lows

Fei Chen and Hans von Storch

Institute of Coastal Research, Helmholtz-Zentrum Geesthacht, Germany

Correspondence should be addressed to Fei Chen; fchen@scsio.ac.cn

Received 22 February 2013; Accepted 2 May 2013

Academic Editor: Lian Xie

The 6-hourly 1948–2010 NCEP 1 reanalyses have been dynamically downscaled for the region of the North Pacific. With a detecting-and-tracking algorithm, the climatology of North Pacific Polar Lows has been constructed. This derived climatology is consistent with the limited observational evidence in terms of frequency and spatial distribution. The climatology exhibits strong year-to-year variability but weak decadal variability and a small positive trend. A canonical correlation analysis describes the conditioning of the formation of Polar Lows by characteristic seasonal mean flow regimes, which favor, or limit, cold air outbreaks and upper air troughs.

1. Introduction

"Polar Low" has been defined as the generic term for all mesoscale cyclonic vortices poleward of main polar front. It should be used for intense maritime mesocyclones with scales less than 1000 km with strong wind speeds [1].

Since the availability of comprehensive observations was supported by satellite imagery, a couple of authors have dealt with space-time statistics of Polar Lows in the North Pacific [2–4]. However, these studies using satellite data cover only a few years of Polar Low occurrences. Also, a combination of subjective detections methods and inhomogeneities in data leads to the possibility that derived trends and variability may not be robust.

A number of authors have applied global reanalysis data for investigating conditions, which are favorable or unfavorable for the formation of Polar Lows and mesocyclones statistics in both Atlantic and Pacific [5, 6]. Kolstad identified low static stability and reverse-wind shear conditions in the 40-year period of ERA-40 reanalyses as favorable conditions. By computing the space-time statistics (i.e., climatology) of favorable conditions for Polar Lows over the North Atlantic, the North-West Pacific and over Southern Ocean, statistics of Polar Low occurrences could be estimated in this indirect manner.

A suitable method for constructing climatology is using long-term dynamical downscaling with regional climate models [7]. Various authors have demonstrated that Polar Lows and other mesoscale windstorms can be described by high-resolution numerical models, such as Fu et al. and Yanase et el. in Japan Sea [8–10]; Bresch et al. in Bering Sea [11]; Businger and Blier in Gulf of Alaska [2, 12]; Chen et al. in North Pacific [13]; Cavicchia and von Storch for "medicanes" in the Mediterranean Sea [14]; and Zahn and von Storch in North Atlantic [7]. Dynamical mechanisms and synoptic conditions of Polar Low formation as well as life cycles have been discussed in various case studies. Reed supported the baroclinic theory in 1979, but he did not reject the possibility of other instabilities for the Polar Low mechanism [15]. The barotropic shear instability has also been put forward to explain the genesis of meso-β-scale Polar Lows over the polar-air mass convergence zone of Japan Sea [16]. High-resolution simulations have also been applied for some idealized experiments to explain mechanisms of Polar Low development such as baroclinicity [10]. A theoretical balanced axisymmetric model has been applied to investigate the wind-induced surface heat exchange intensification mechanism in Polar Low development by Gray and Craig [17]. Various case studies indicate that usually several mechanisms together lead to the formation of Polar Lows [18–20]. A recent study also pointed out that Polar Lows influence the large-scale ocean circulation and deep water transport over the Nordic sea [21].

In this paper, we employ the method developed by Zahn and von Storch [7, 22] to dynamically downscale the gridded large-scale synoptic fields, as provided by large-scale component of reanalyses—here: NCEP 1 [23]. In a first step, we have shown in a series of cases that downscaling generates Polar Lows with sufficient accuracy [13]. Now, in this study, a regional climate model (RCM) has been run continuously for 63 years during which the NCEP 1 reanalyses are available. During the integration, the model is constrained in its large-scale components to be similar to the driving NCEP reanalysis, using the method of spectral nudging [24]. The output of this multidecadal simulation is used for investigating trends and variability of Polar Low occurrences in the North Pacific and their linkage to the seasonal mean large-scale circulation situations over the last 63 years.

We are sometimes confronted with the request that such an analysis should result in new insights into the dynamics of Polar Low formation and life cycles. However, this is not the intention of the present study. Such case studies have been done in many cases (as stated previously), and we do not intend to extend this large number of dynamical analyses. Instead, we are interested in space-time statistics, including the conditioning by large-scale dynamical configurations, of Polar Lows, in particular, on the differences between regions and years and decades, and in systematic changes. Thus, the present analysis does not contribute to dynamical meteorology but to climatology.

In Section 2, we describe briefly the model and the detection-and tracking methodology used in this study. This methodology differs a bit from the previous study of Chen et al. [13] as well as the North Atlantic study by Zahn and von Storch [22]. The derived statistics of the formation of Polar Lows in space and time is the subject of Section 3. In Section 4, we determine linkages of seasonal mean large-scale flow in the North Pacific and the number of storms formed in different subregions of the North Pacific. The paper is concluded with a discussion and the recapitulation of major results finally in Section 5.

2. Data and Methodology

The RCM we applied in this study is the COSMO-CLM 4.8 (COSMO model in CLimate Mode) [25, 26]. This model is the climate version of the operational weather prediction model of the Deutscher Wetterdienst (German National Weather Service) and the COnsortium for Small-scale MOdeling (COSMO), adapted to climate simulation purposes by the CLM-Community (http://www.clm-community.eu/). The model domain covers the whole North Pacific (Figure 3(b)). We used NCEP 1 reanalysis data as initial and lateral boundary conditions. In particular, the sea surface temperature (SST) and sea ice extent were prescribed as lower boundary according to the NCEP 1 reanalyses. Spectral nudging [24] of tropospheric wind components was applied for enforcing the NCEP large-scale situation in the model region in order to prevent COSMO-CLM from significantly deviating from the analyzed large-scale state. The nudging is applied at 850 hPa and above, with the nudging becoming stronger with height. Only spatial scales larger than 800 km are constrained; smaller features are unconstrained. A rotated grid with 0.4° grid resolution and 220 and 80 points is employed for the longitudinal and latitudinal grid map. The 8-grid sponge zone is introduced to avoid reflection of waves at the boundaries. Boundary data is prescribed by this zone with decreasing influence for the inner grid points. The simulation results from the sponge zone are not usable for further analysis. The number of vertical levels is 40. The simulation period began on January 1, 1948 and ended on December 31, 2010. For further details about the model setup, refer to Chen et al. [13].

An automatic detection-and-tracking procedure was applied to determine the presence and tracks of Polar Lows in the North Pacific. The detection procedure searches for the minima in the band-pass filtered mean sea level pressure (MSLP) fields and concatenates the minima in consecutive time steps to tracks. Along these tracks, the fulfillment of further criteria is requested for categorizing an event as Polar Low:

(1) strength of the minimum band-pass filtered MSLP: ≤ -2 hPa once along the track;

(2) wind speed: $\geq$13.9 m/s once along the track;

(3) sea surface versus mid troposphere temperature difference: SST-$T_{500\,\mathrm{hPa}} \geq 39$ K;

(4) average direction of the track: a north-to-south component;

(5) limits to allowable adjacent grid boxes. No land: those tracks are excluded when over 50% of the positions near the coastal grid boxes along the track.

When the minimum of the band-pass filtered MSLP along these tracks decreases below -6 hPa once and there are no coastal grid boxes close to that location, a Polar Low is recorded irrespective of the other criteria.

This is mostly identical to the North Atlantic setting of Zahn and von Storch [22], but some parameters (like the air-sea temperature difference) have been modified in order to meet the conditions in the North Pacific better [13]. However, we used now a cosine (discrete cosine transforms: DCT) band-pass filter of Denis et al. [27] instead of the digital filter used by Zahn and von Storch [22], after Xia et al. [28] pointed out the superiority of the first one. DCT is more precise in scale separation than the original digital filter.

Some Polar Lows in the North Pacific move on average in zonal direction, like the case of 22nd of March 1975 described by Chen et al. [13]. Therefore, the request for a north-to-south movement may be too strict. However, without this criterion, also smaller baroclinic storms may be categorized as Polar Lows. In order to examine the significance of this zonal movement criterion for variability and long-term trend, we did the analysis with both criteria, with and without N-S direction criterion (see Figure 1).

3. Results: Space Time Statistics of Tracks

Polar Lows are a phenomenon forming in the "cold season;" therefore, the "Polar Low season" (PLS) in the North Pacific is

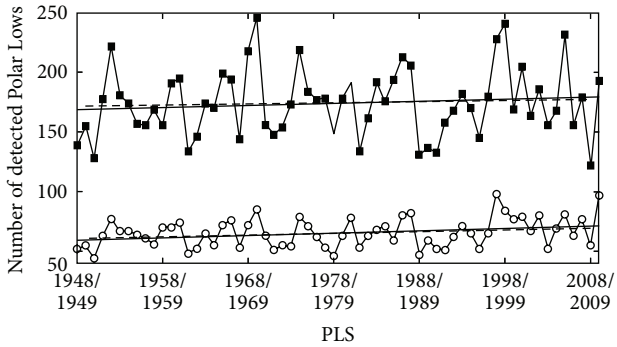

Figure 1: Number of detected Polar Lows in the North Pacific per Polar Low season (October to April). Top curves: the detected number of Polar Lows without N-S criterion (marked with ■). The solid line represents the trend from 62 PLSs, from 1948/1949 to 2009/2010, which is 0.17 cases/year; the dashed line represents the trend from only 60 years, from 1949/1950 to 2008/2009, which is 0.09 cases/year. Bottom curves: the detected number of Polar Lows with N-S criterion (marked with ◯). The solid line represents the trend from 1948/1949 to 2009/2010, which is 0.2 cases/year; the dashed line represents the trend from 1949/1950 to 2008/2009, which is 0.14 cases/year.

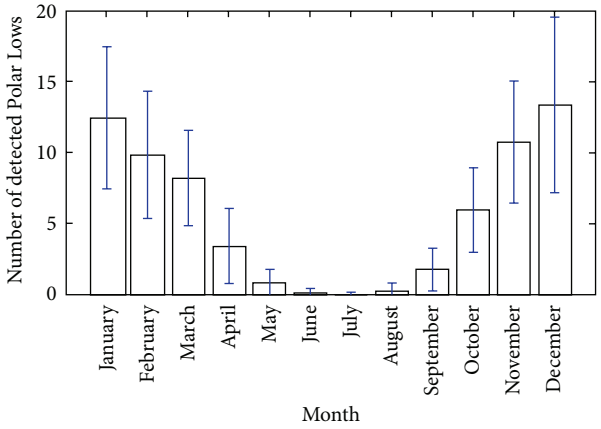

Figure 2: Number of detected Polar Lows in an average calendar month for the whole 62 PLSs. Tracking with N-S criterion. The error bar is the standard deviation of Polar Low variance in each month during the 62 PLSs.

defined as the time from October through April the following year. This is a bit different from Zahn and von Storch [7] in the case of the North Atlantic: they count the PLS from July to next June. As we know, there are few Polar Lows in summer (see Figure 1); the Polar Low season is addressed by the first and second year; for example, the PLS 1950/1951 begins in October 1950 and ends in April 1951. The statistical analysis excluded the first half year of 1948 and last half year of 2010, as they represent only part of a Polar Low season. So we have 62 PLSs, with the first from October 1948 to April 1949 and the last from October 2009 to April 2010.

Figure 1 shows the time series of the number of detected Polar Lows per PLS both without and with N-S criterion. In all the following analyses, the criterion of an average movement with a North-to-South component is applied.

When looking only for cases *without a directional constraint of the movement,* a total of 10812 Polar Lows were detected by the tracking algorithm during the 62 Polar Low seasons. On average, 174 Polar Lows were found per PLS, with a strong year-to-year variability indicated by a standard deviation of 29 (±17% of the long-term mean). The decadal variability is weak. The overall trend, from the first PLS in 1948/1949 to the last PLS in 2009/2010, in the frequency of Polar Low is positive with 0.17 cases/PLS, which yields about 11 Polar Lows more in the end than in the beginning of the series (11 cases correspond to 6% of the long-term mean). We have to point out that the slope of the trend depends on the number of cases of the first and last PLSs. When disregarding the last and the first PLSs, the trend of Polar Lows from PLS 1949/1950 to 2008/2009 is smaller, with only 0.09 cases/PLS.

For the result *with the N-S criterion,* fewer Polar Lows are detected, namely, only 4052 Polar Lows during the 62 Polar Low seasons. On average, 65 Polar Lows were found per PLS, with a strong year-to-year variability indicated by a standard deviation of 12 (±18% of the long-term mean). Maximum number of detected cases is found in PLS 1997/1998 with 98 cases; the minimum number is in PLS 1950/1951 with 44 cases. The overall trend, from the first PLS in 1948/1949 to the last PLS in 2009/2010, in the frequency of Polar Low is positive with, on average, additional 0.2 cases per PLS, which yields about 12 Polar Lows more in the end than in the beginning of the series (corresponding to 21% of the mean total). The trend of Polar Lows from PLS 1949/1950 to 2008/2009 is positive with 0.18 cases/PLS. When calculating 10 trends from 1948/1949–2009/2010, 1949/1950–2008/2009 to 1957/1958–2000/2001, the mean trend is 0.16 cases/PLS; the standard deviation of these 10 trends is 0.03/PLS, so that the estimate of the trend appears relatively insensitive to the early and late values.

There is no acceleration of a trend towards the end of the time series. Furthermore, the trend seems mostly uniform and rather small. According to the prewhitened Mann-Kendall trend test [29], the 62 PLSs trend of the number of detected Polar Low is significant (5% risk; result not shown) for the configurations with directional constraining, but insignificant when examining the curve derived without directional constraint.

The annual cycle of monthly numbers of detected Polar Lows with N-S criterion exhibits the highest frequency in winter with maxima in December and January and almost no Polar Low activity in summer (Figure 2), consistent with the observation that Polar Lows form in the cold season. Furthermore, we determined the annual cycle of the days with Polar Lows during the same time period as Businger [2], namely, 1975–1983, and found our results consistent with Businger's results. The results differ with respect to a secondary peak in January in our 1975–1983 climatology but in February in Businger's climatology (Figure not shown). In view of the very different methods applied by us and by Businger, namely, satellite observations versus downscaled reanalyses, the differences may be considered acceptable. When examining the set of Polar Lows derived without the directional constraint, a very similar annual cycle, apart of a uniform bias in the magnitude, is found (not shown).

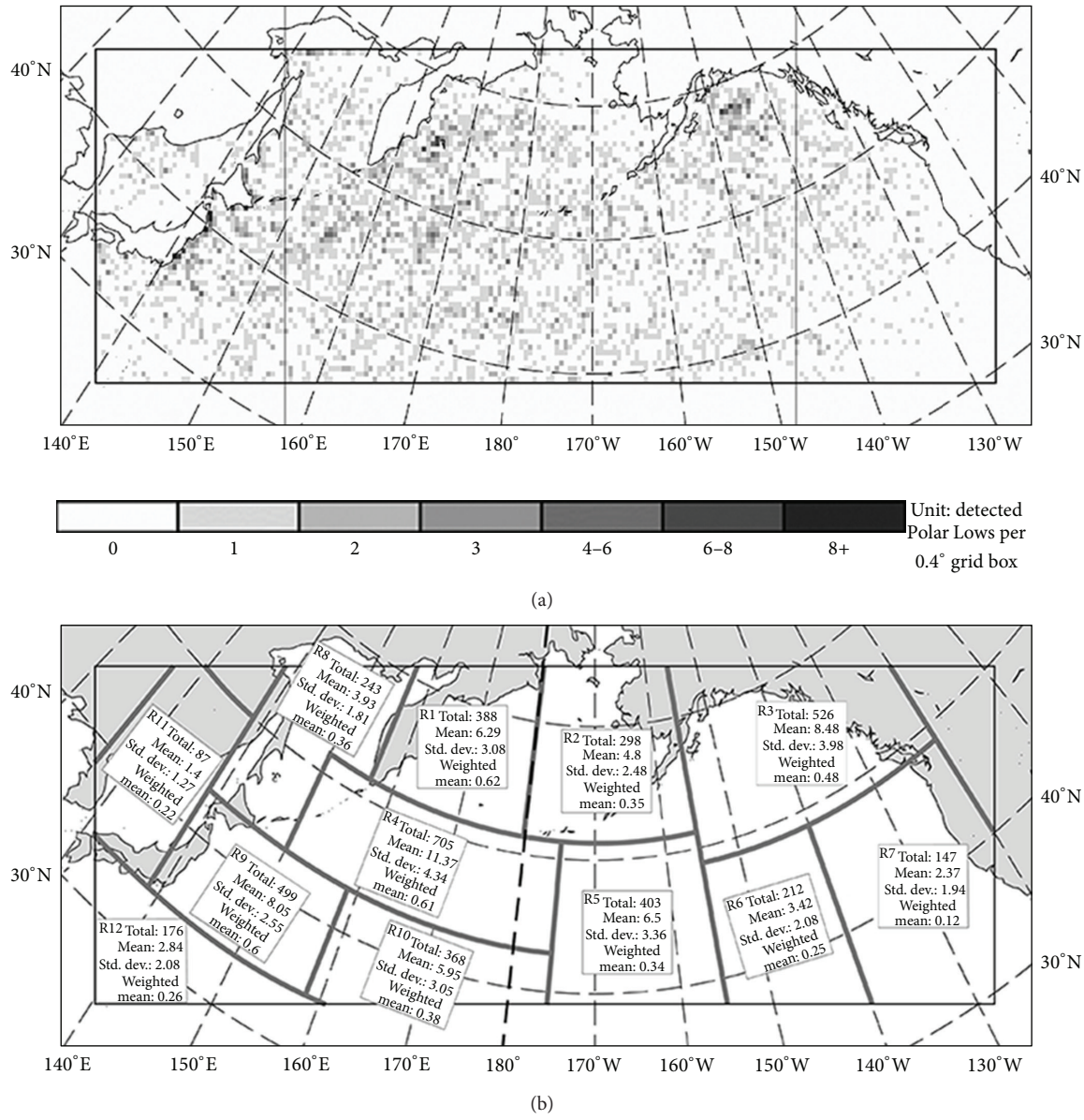

Figure 3: (a) Density distribution of first appearance of Polar Lows. Unit: detected Polar Lows per 0.4° grid box. (b) Subregions R1–12, for which statistics of Polar Lows were aggregated: the total number, the mean number per Polar Low season (mean), year-to-year standard deviation (std. dev.), and number of Polar Lows per number of no land grid points in the subregion (weighted mean).

There is no suggestion in the literature about the general number and trend of Polar Lows in the North Pacific that we should expect. Therefore, we find it difficult to decide if the directional constraint is really helpful or not. Clearly, the total number depends strongly on this criterion, but the overall trends are similar in both cases. This indicates that the N-S criterion does not much influence the general characteristic of long-term trend. The correlation coefficient between the two curves is 0.82, in both cases, with and without N-S criterion. Under the consideration that the N-S criterion is more reasonable from the dynamical view of Polar Low generation, we have chosen the result with N-S criterion for further discussions.

The spatial distribution of Polar Low density is shown in Figure 3(a). The Polar Low density counts the frequency per grid box of a first detection of a Polar Low. Highest densities are found in the region east of Japan in accordance with the results of Yarnal and Henderson [4]. By analysing defense meteorological satellite program (DMSP) infrared imagery from 7 winter seasons, Yarnal and Henderson concluded that the most active Polar Low cyclogenesis takes place in the western extratropical North Pacific. Our peak area of Polar Low density is just off the east coast of Japan Island, while Yarnal and Henderson's result has its peak a little north, near the island of Hokkaido. In both analyses, there is much less Polar Low activity in the eastern North Pacific than in the western part.

Yarnal and Henderson [4] pointed out that there are two bands that extend from northern Japan through the Kamchatka Peninsula into the western Bering Sea; another

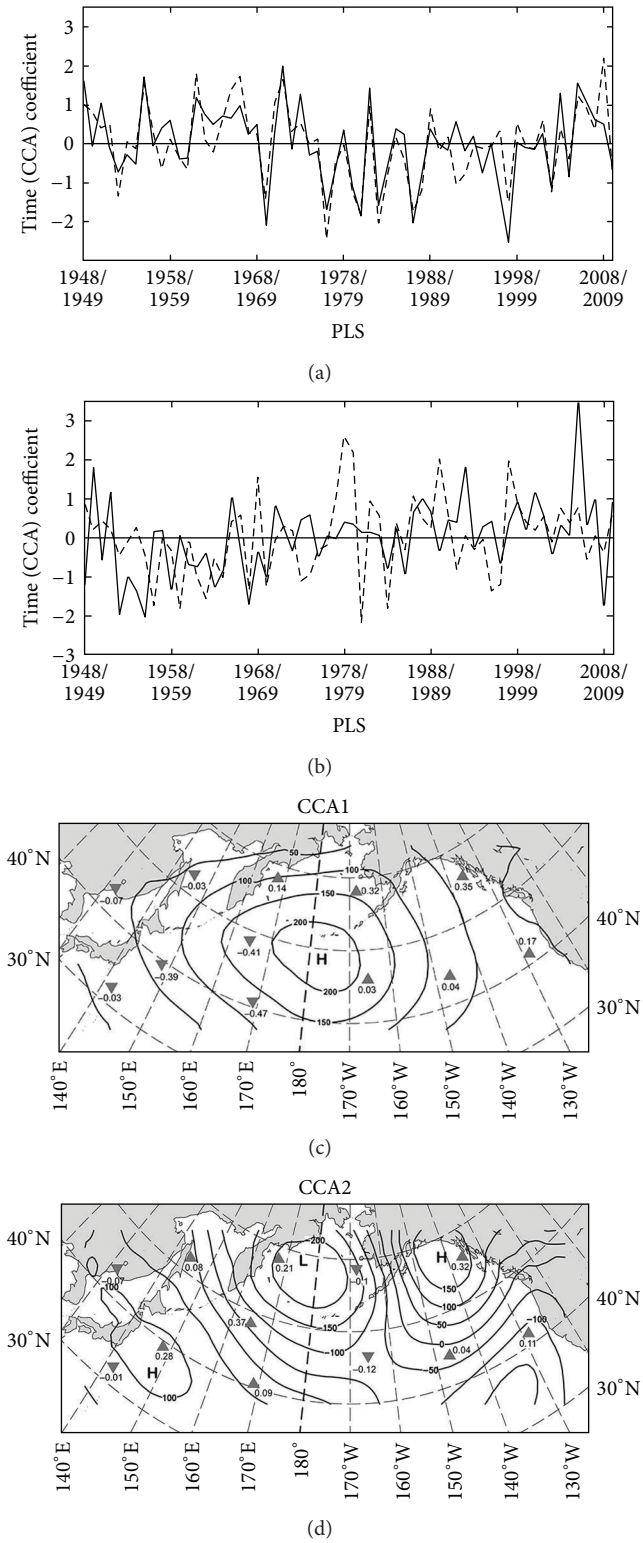

Figure 4: ((a), (b)) First two canonical correlation coefficient time series (dashed lines represent the Polar Low occurrence and solid lines represent the MSLP pattern) and ((c), (d)) corresponding canonical correlation patterns between regional time series of Polar Low occurrences per PLS in subregions R1–R12 ($\triangle$ for positive values, $\triangledown$ for negative values) and mean sea level pressure fields in Pa. The first CCA pair ((a) and (c)) shares a correlation coefficient of 0.89. The second CCA pair ((b) and (d)) shares a correlation of 0.72.

one extends eastward into the open waters of the North Pacific to just east of the international date line. Such two bands are also present in our climatology of the first detected position of the Polar Lows. Additionally, we find also high values for the Gulf of Alaska, where Yarnal and Henderson have detected only "a couple of small, weak pockets of formation."

In order to compare the information of Polar Lows over different regions of North Pacific, we divided the domain into 12 subregions (Figure 3(b)). Some of the subregions are based on the oceanographic feature, such as the Bering Sea (R1 and R2; they are divided by the international date line), the Gulf of Alaska (R3), the Okhotsk Sea (R8), and the Japan Sea (R11). The others are dependent on the climatology cyclogenesis by Yarnal and Henderson [4]. The two bands with the highest frequency of Polar Low occurrence are referred to as R4 and R9. The eastern North Pacific with much less activity is represented by R5, R6, and R7. R10 and R12 are the subregions in the south with seldom distribution. For the different regions in Figure 3(b), small trends and high year-to-year variability for Polar Low frequency were found. Some regions (especially for R1, R3, and R4 with high density) have a higher year-to-year standard deviation than others (R6, R7, R8, R11, and R12) (not shown).

4. Linkage to Large-Scale Pressure Patterns

We begin with investigating how *mean sea level pressure (MSLP)* fields, averaged across a Polar Low season, are related to the distribution of the numbers of Polar Low occurrences in that season. Here, we emphasize that the analysis is not about short-term synoptic situation or the instantaneous air pressure field directly related with the probability of a Polar Low to form. Instead, we compare two statistics during the same Polar Low season, namely, the geographical distribution of Polar Lows, aggregated to the twelve subregions shown in (Figure 3(b)) and the gridded time-mean MSLP field.

The link between MSLP and the number of Polar Lows is done through a canonical correlation analysis (CCA [30]). CCA is a method for calculating correlation structures between two fields of variables. To reduce noise in each set, we projected the full fields on the first 5 empirical orthogonal functions (EOFs) of the Polar Low time series (representing 77% of the variance) and of the PLS-mean MSLP (87% of the variance). Prior to the CCA, the multiyear mean field is subtracted; that is, the analysis is done with anomalies.

Figure 4 shows the resulting time series and spatial patterns of the two most important linkages between the regional distribution of Polar Lows and the time-mean MSLP field.

The first canonical pattern (CCA1, Figure 4(c)) describes a unipolar pressure distribution. When the CCA coefficient is positive, then, on average, there will be a west-eastward cold air flow across the Bering Sea and south-eastward across the Gulf of Alaska and, consistently, more Polar Lows in that region. These time-mean flows are characteristic for more or less, short-term marine cold air outbreaks in these regions. It is indicated that there is a close relationship between Polar Low formation and the presence of a trough in winter over

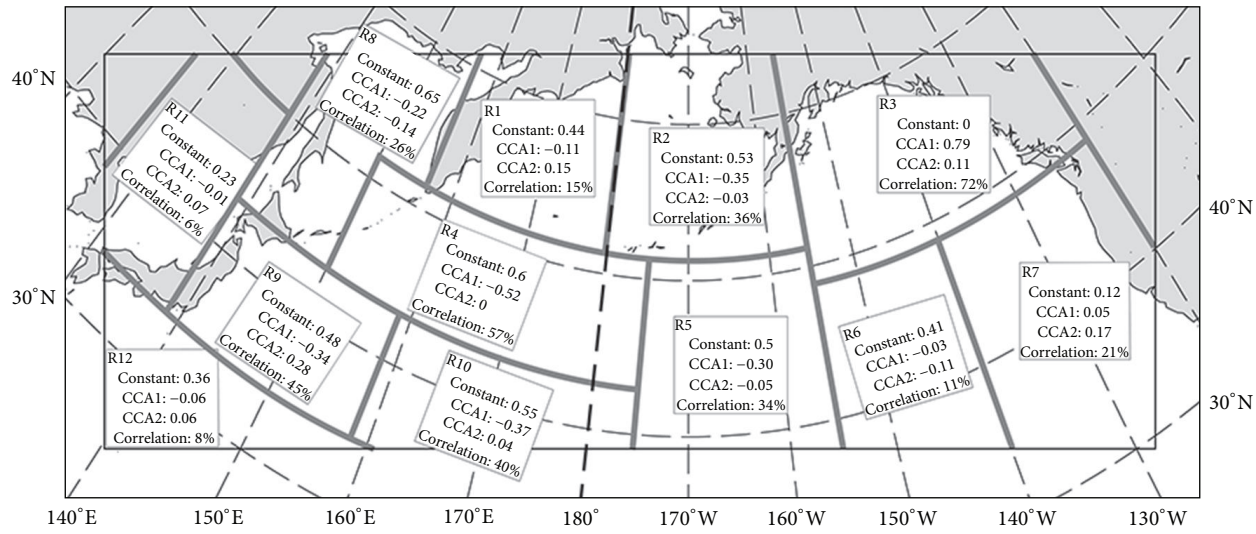

FIGURE 5: Result of multiple regression analyses of the first two CCA coefficients on the number of Polar Lows in subregions R1–12: coefficient a_0 (constant), a_1 (connected to CCA1), a_2 (connected to CCA2), and the correlation of number of Polar Lows and trough regressions estimated number of Polar Lows.

East Asia and the nearby North Pacific [2]. The strong land-sea thermal contrast along the marginal ice zone pulls cold continental polar or Arctic air over the Bering Sea and the Japan Sea. The relatively warm waters in the open ocean lead to the formation of Polar Lows through convective instability and baroclinicity.

The time series of canonical correlation coefficient (Figures 4(a) and 4(b)) explains the significance of the two fields of variables over the 62 PLSs. Dashed lines represent the pattern of Polar Low occurrence over the 12 subregions; meanwhile, the solid lines represent the MSLP pattern. When examining the time series in Figure 4(a), it is evident that CCA1 dominates the Polar Low seasons in 1954/1955, 1971/1972, and 1981/1982.

The second canonical pattern (CCA2, Figure 4(d)) shows a bipolar pressure distribution—there is a negative anomaly (below −2 hPa) on the Bering Sea at the same time as two positive anomalies on the Gulf of Alaska and Japan Island (over 1 hPa). Consequently, there will be a south-eastward time-mean flow starting from Siberia, across the Sea of Okhotsk, and then the southwest of Bering Sea where, in subregion R4, consistently more Polar Lows are detected on average. A time-mean pressure contrast of about 3 hPa between the Bering Sea and the west and east part of North Pacific (the region around Japan Island and the west coast of North American continent) is associated with 0.2 to 0.3 more Polar Lows per PLS in the corresponding regions (R1, R3, R4, and R9).

By examining the time series in Figure 4(b), we found that CCA2 dominates the Polar Low seasons of 1951/1952, 1975/1976, and 1998/1999, which means there were more Polar Lows in regions R1, R3, R4, and R9; the negative signs in 1949/1950 and 1978/1979 point to remarkably less Polar Lows in these regions.

To determine the relative importance of the two CCA patterns, we have built for each subregion R1–R12 a regression model, of the form $\mathrm{PL}_i(t) = a_{0,i} + a_{1,i} \times \mathrm{CCA}_1(t) + a_{2,i} \times \mathrm{CCA}_2(t) + \varepsilon_i$. Here, $\mathrm{PL}_i(t)$ is the number of Polar Lows in season t and in subregion i, $a_{0,i}$, $a_{1,i}$, and $a_{2,i}$ are the regression coefficients, which are determined by a least square fit, $\mathrm{CCA}_1(t)$ and $\mathrm{CCA}_2(t)$ are the CCA coefficients of patterns 1 and 2 in season t, and ε_i is the residual, the unexplained part. In Figure 5, we list the regression coefficients and the correlation between the number of Polar Lows and through these regressions estimated number of Polar Lows for every subregion.

The two series, $\mathrm{CCA}_1(t)$ and $\mathrm{CCA}_2(t)$, are about equally important, when counting how often $|a_1(t)| > |a_2(t)|$. They are particularly successful to describe the variability in all but one of the highest frequency occurrence area which we showed in Figure 3—for subregions 3, 4, 9, and 10, the correlation is over 40%, while in the far eastern (subregion 6 and 7) and western (11 and 12), the correlations are less than 25%. When comparing with Figure 3(b), we see that the frequency of occurrence of Polar Lows in the subregions 6, 7, 11, and 12 is relatively low: the mean number of Polar Lows in 7, 11, and 12 together is 6.61 Polar Lows per PLS, while the occurrences in each of subregions 3, 4, and 9 separately are stronger than this intensity, namely, 8.48, 11.37, and 8.05 Polar Lows per PLS. In subregion 1, frequency of occurrence is relatively high (6.29 Polar Lows per PLS) but the correlation is low (15%).

Next, we examine the link to *time-mean distribution throughout the troposphere*. Therefore, we derive associated correlation patterns [30] to describe the linkage between Polar Low occurrence and geopotential height in different pressure levels (Figure 6).

Associated correlation patterns are designed to describe the relationship between time series of an "index" variable and a physical field. By calculating the correlation coefficient between the time series of CCA coefficient for Polar Low occurrence pattern (dashed lines in Figures 4(a) and 4(b))

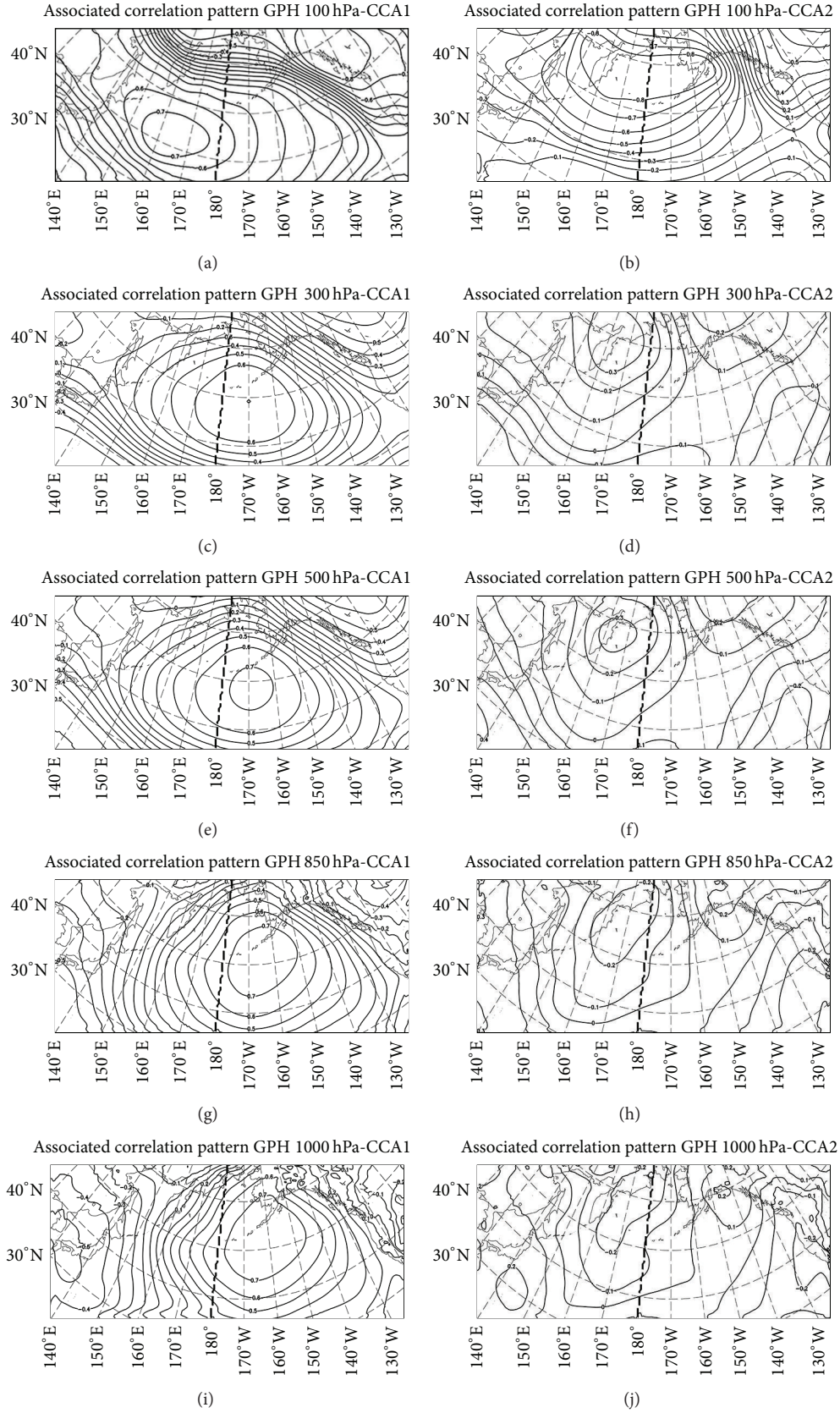

Figure 6: Associated correlation patterns between time series of geopotential height over 62 PLSs and time coefficient of the Polar Low occurrence from the first two CCA patterns (1st CCA pair, left column, 2nd right column). From top to bottom, 100, 300, 500, 700, 850, and 1000 hPa. All variables are averaged across a Polar Low season, that is, from October to April.

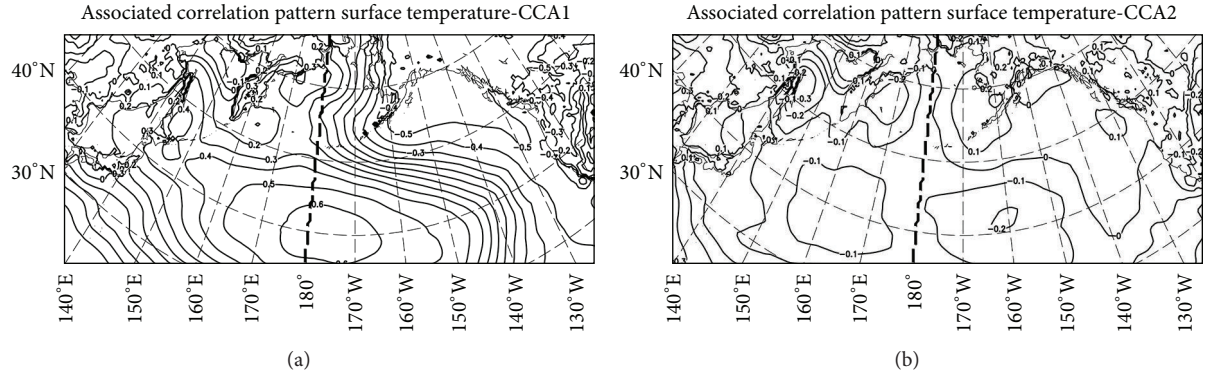

Figure 7: Associated correlation patterns between time series of ocean surface temperature anomalies over 62 PLSs and time coefficient of the Polar Low occurrence from the first two CCA patterns (1st CCA pair, left column, 2nd right column). All variables are averaged across a Polar Low season, that is, from October to April. The surface temperature was taken from the NCEP1 reanalysis data, over the ocean. In case of no ice, it indicates the sea surface temperature (SST); else, it indicates the ice surface temperature.

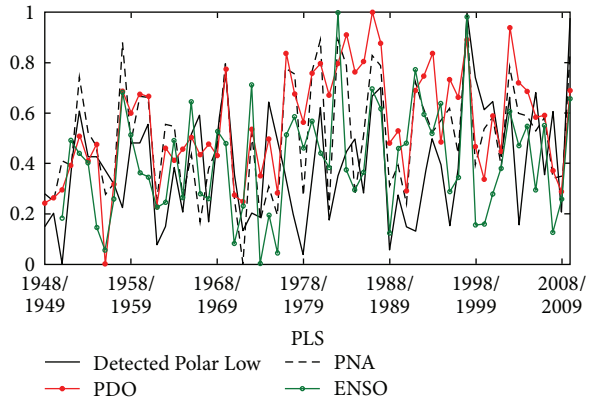

Figure 8: Time series of normalized detected Polar Low number (black line), PDO index (red, marked with o), PNA index (black, dashed), and ENSO index (green, marked with o). The indices are determined as average across the Polar Low seasons.

and the time series of geopotential height anomalies for each grid point on each level, we derive typical configurations on every pressure level associated with the two Polar Low patterns shown in Figures 4(c) and 4(d) (the triangles). The anomalies were formed by subtracting the time-mean fields for the 62 considered Polar Low seasons.

The maps of correlation coefficients present similar patterns to the corresponding MSLP field of the CCA results (Figures 4(c) and 4(d); isolines). It indicates that the relationship between the atmosphere circulation and Polar Low occurrence is mostly barotropic, even if in the lower stratosphere of 100 hPa the pattern is somewhat shifted. The cold flow which is inducing the Polar Low occurrence is uniform throughout the troposphere, from sea level to the upper troposphere and the lower stratosphere.

On the upper levels at 100, 300, 500, and 700 hPa, the isolines are smoother. On the lower level at 850 and 1000 hPa, the solid lines are more wiggly: the orography and sea surface temperature attain a stronger influence on the generation of more or less Polar Lows.

In order to investigate the link with *sea surface temperature (SST)* and respective sea ice temperature in case of ice, a pair of associated correlation patterns is presented (Figure 7) to describe the linkage between the CCA-time series of Polar Low occurrence (dashed lines in Figures 4(a) and 4(b)) and the surface temperature. These temperatures were taken from the same NCEP1 reanalysis, which was used to force the regional model simulation.

Both associated correlation patterns of SST are consistent with the flow patterns of the CCA result. Temperatures tend to be lower, where more cold air is advected, and higher than on average, when the flow advects less cold or more warm air. Previous modeling studies have shown that the mechanism behind these patterns is that of an oceanic response to anomalous atmospheric flow [31, 32], first suggested by Bjerknes [33] for the Atlantic. We conclude that anomalous mean flow is responsible for both, the formation of anomalous SST as well as the formation of more, or less Polar Lows, in the North Pacific.

In order to investigate the *large-scale dynamical environment* of changing Polar Low occurrences, we analyze the correlation between the time series of detected Polar Low number in the different subregions and several climate variability indexes, namely, the Pacific decadal oscillation (PDO [34–36]), Pacific-North American teleconnection pattern (PNA [37]), and El Niño/La Niña-Southern oscillation (ENSO multivariate ENSO index; see http://www.esrl.noaa.gov/psd//people/klaus.wolter/MEI/table.html). The time series for the normalized Polar Low numbers PDO, PNA, and ENSO index are shown in Figure 8.

The correlation coefficient of detected Polar Low number in simulation area with PDO index is 0.39, with PNA index is 0.45, and with ENSO index is 0.22. It indicates that the Polar Low formation over the North Pacific has the highest relationship with PNA and PDO; there is limited influence by ENSO.

Multiple regression analyses of the number of Polar Lows in the 12 subregions (Figure 3(b)) with the time-mean circulation indices for PDO, PNA, and ENSO reveal which regions are mostly affected by the state of the three circulation systems. The regressions results are listed in Figure 9 for every subregion as well as the correlations between the number of Polar Lows and the through regression estimated number of

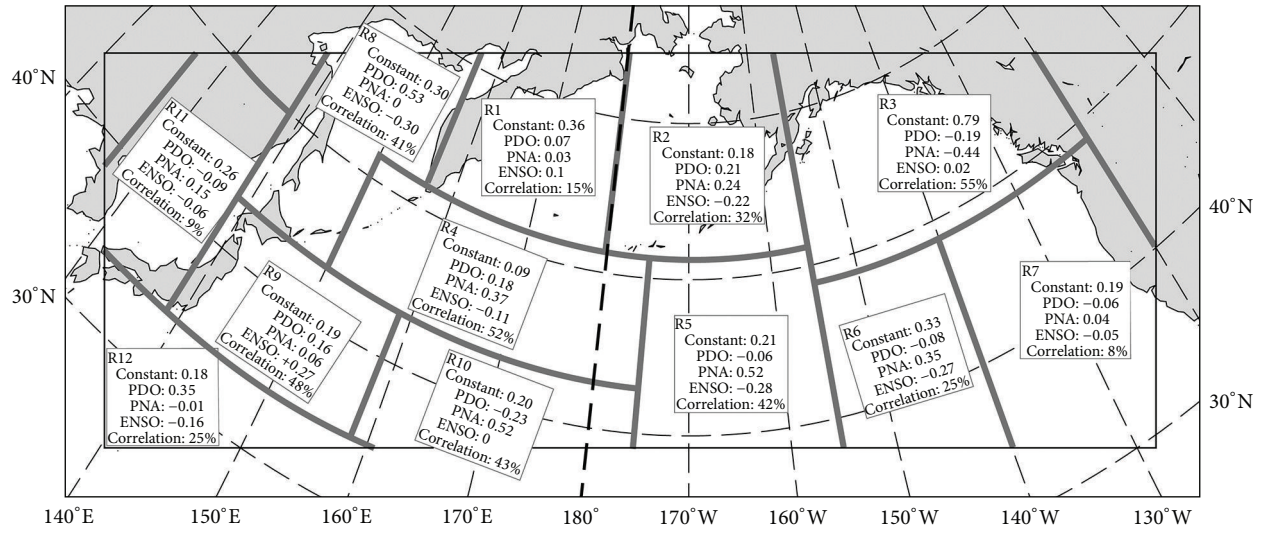

Figure 9: Results of multiple regression analyses of number of Polar Low subregions R1–12: the constant parts and the coefficients associated with the PLS time-mean circulation indices PDO, PNA, and ENSO.

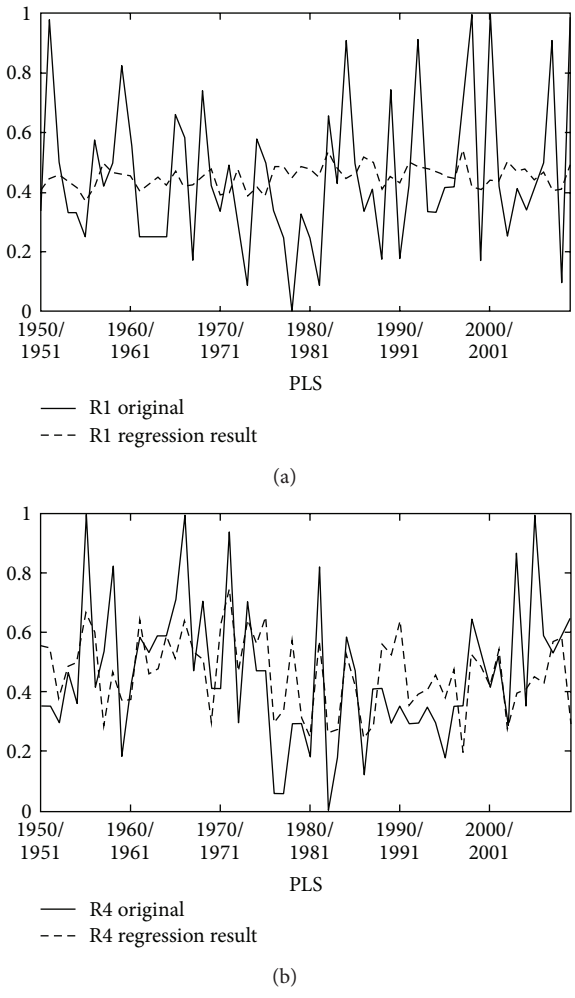

Figure 10: Multiple regression of PLS-time mean circulation indices PDO, PNA, and ENSO on the number of Polar Lows in two of the 12 subregions shown in Figure 3—top: R1, bottom: R4.

Table 1: Result of multiple regression analysis of the first two time series of MSLP patterns of CCA between MSLP and Polar Low occurrence and of PLS time mean circulation indices PDO, PNA, and ENSO.

	Constant	PDO	PNA	ENSO	Correlation
CCA1	0.07	0.19	0.54	−0.01	71%
CCA2	0.48	−0.03	0.36	−0.37	26%

Polar Lows. Obviously, the indices are not independent, so that there is no strict separation of the effect of the circulation systems. As an example, the result of the regression is shown for two subregions in Figure 10—one is R1 in the North close to the date line, with a very low correlation of only 15%, and the other is R4 south of R1 in the central part of the North Pacific, with the largest correlation, namely, 55%. Obviously, the circulation indices cannot be associated with year-to-year variability in R1, while the skill of the indices in describing this variability is remarkable in R4.

We find only two regions, R3 and R4, where the total influence of the indices amounts to a correlation of more than 50%. R3 is in the Northeast, south of Alaska, while R4 is at middle latitudes west of the date line; in both cases, PNA is associated with the largest coefficient, which is consistent with the pattern of PNA (not shown). A weak link, as expressed by a correlation of 30% or less, is found for R1, R6, R7, R11, and R12, all subregions at the boundaries of the model domain.

To characterize the variability of the CCA patterns and the large-scale state indices of PDO, PNA, and ENSO, we have also established regression models. They relate the time series of the MSLP pattern with the three indices. The success and relative importance of the three indices are summarized in Table 1. Additionally, the correlations between the time series of MSLP pattern and the one estimated through the regression are listed.

The first CCA pattern is strongly linked to, primarily, PNA and also PDO (which are of course not independent) but

hardly to ENSO; this is different for the second pattern, which is described as being negatively linked to ENSO, equally strongly linked to PNA but hardly to PDO. The overall link is much stronger for the first pattern (as indicated by a correlation of 71%), while the link for the 2nd pattern is weak (correlation of 26%).

5. Summary and Outlook

For the first time, a multidecadal climatology, including trends, of Polar Low formation in the North Pacific has been constructed. Because of an insufficient database of local observations and homogeneous high-resolution analyses, a dynamical downscaling strategy has been employed, following the concept developed by Zahn and von Storch [22].

The main result is the presence of large interannual variability in 1948–2010, but little decadal variability of Polar Low occurrences and positive long-term changes in the North Pacific region. No obvious change was detected in recent decades, which indicates that the large natural variability in the region is still dominating over possible effects of global warming.

The tendency of forming more, or less, Polar lows has been related to the time-mean circulation in the North Pacific, in terms of mean sea level pressure and geopotential height throughout the troposphere. Anomalous flows from cold surfaces were found to support the large-scale synoptic environment of Polar Low formation. Two major patterns are detected, which are correlated with the variations described by the indices of PDO, PNA, and, to a lesser extent, ENSO.

Acknowledgments

The work was done with the support of the Chinese Scholarship Council CSC, and it is a contribution to the Helmholtz Climate Initiative REKLIM (Regional Climate Change), a joint research project of the Helmholtz Association of German Research Centers. The authors thank Beate Gardeike for preparing most of the diagrams. The technical and scientific support, the various comments and suggestions by Dr. Beate Geyer and Dr. Matthias Zahn have greatly improved this paper.

References

[1] G. Heinemann and C. Claud, "Meeting summary: report of a workshop on "theoretical and observational studies of polar lows" of the European Geophysical Society Polar Lows Working Group," *Bulletin of the American Meteorological Society*, vol. 78, no. 11, pp. 2643–2658, 1997.

[2] S. Businger, "The synoptic climatology of polar-low outbreaks over the Gulf of Alaska and the Bering Sea," *Tellus A*, vol. 39, no. 4, pp. 307–325, 1987.

[3] K. Ninomiya, "Polar/comma-cloud lows over the Japan Sea and the Northwestern Pacific in Winter," *Journal of the Meteorological Society of Japan*, vol. 67, pp. 83–97, 1989.

[4] B. Yarnal and K. G. Henderson, "A climatology of polar low cyclogenetic regions over the North Pacific-ocean," *Journal of Climate*, vol. 2, no. 12, pp. 1476–1491, 1989.

[5] A. Condron, G. R. Bigg, and I. A. Renfrew, "Polar mesoscale cyclones in the northeast Atlantic: comparing climatologies from ERA-40 and satellite imagery," *Monthly Weather Review*, vol. 134, no. 5, pp. 1518–1533, 2006.

[6] E. W. Kolstad, "A new climatology of favourable conditions for reverse-shear polar lows," *Tellus A*, vol. 58, no. 3, pp. 344–354, 2006.

[7] M. Zahn and H. von Storch, "A long-term climatology of North Atlantic polar lows," *Geophysical Research Letters*, vol. 35, no. 22, Article ID L22702, 2008.

[8] G. Fu, H. Niino, R. Kimura, and T. Kato, "A polar low over the Japan Sea on 21 January 1997. Part I: observational analysis," *Monthly Weather Review*, vol. 132, no. 7, pp. 1537–1551, 2004.

[9] W. Yanase, G. Fu, H. Niino, and T. Kato, "A polar low over the Japan Sea on 21 January 1997. Part II: a numerical study," *Monthly Weather Review*, vol. 132, no. 7, pp. 1552–1574, 2004.

[10] W. Yanase and H. Niino, "Dependence of polar low development on baroclinicity and physical processes: an idealized high-resolution numerical experiment," *Journal of the Atmospheric Sciences*, vol. 64, no. 9, pp. 3044–3067, 2007.

[11] J. F. Bresch, R. J. Reed, and M. D. Albright, "A polar-low development over the bering sea: analysis, numerical simulation, and sensitivity experiments," *Monthly Weather Review*, vol. 125, no. 12, pp. 3109–3130, 1997.

[12] W. Blier, "A numerical modeling investigation of a case of polar airstream cyclogenesis over the Gulf of Alaska," *Monthly Weather Review*, vol. 124, no. 12, pp. 2703–2725, 1996.

[13] F. Chen, B. Geyer, M. Zahn, and H. von Storch, "Toward a multidecadal climatology of North Pacific polar lows employing dynamical downscaling," *Terrestrial, Atmospheric and Oceanic Sciences*, vol. 23, pp. 291–301, 2012.

[14] L. Cavicchia and H. von Storch, "The simulation of medicanes in a high-resolution regional climate model," *Climate Dynamics*, vol. 39, no. 9-10, pp. 2273–2290, 2012.

[15] R. J. Reed, "Cyclogenesis in polar airstreams," *Monthly Weather Review*, vol. 107, no. 1, pp. 38–52, 1979.

[16] M. Nagata, "Meso-β-scale vortices developing along the Japan-Sea polar- airmass convergence zone (JPCZ) cloud band: numerical simulation," *Journal Meteorological Society of Japan*, vol. 71, no. 1, pp. 43–57, 1993.

[17] S. L. Gray and G. C. Craig, "A simple theoretical model for the intensification of tropical cyclones and polar lows," *Quarterly Journal of the Royal Meteorological Society*, vol. 124, no. 547, pp. 919–947, 1998.

[18] S. Businger, "The synoptic climatology of polar low outbreaks," *Tellus A*, vol. 37, no. 5, pp. 419–432, 1985.

[19] T. E. Nordeng, "A model-based diagnostic study of the development and maintenance mechanism of two polar lows," *Tellus A*, vol. 42, no. 1, pp. 92–108, 1990.

[20] J. Mailhot, D. Hanley, B. Bilodeau, and O. Hertzman, "A numerical case study of a polar low in the Labrador Sea," *Tellus A*, vol. 48, no. 3, pp. 383–402, 1996.

[21] A. Condron and I. A. Renfrew, "The impact of polar mesoscale storms on northeast Atlantic Ocean circulation," *Nature Geoscience*, vol. 6, pp. 34–37, 2013.

[22] M. Zahn and H. von Storch, "Tracking polar lows in CLM," *Meteorologische Zeitschrift*, vol. 17, no. 4, pp. 445–453, 2008.

[23] E. Kalnay, M. Kanamitsu, R. Kistler et al., "The NCEP/NCAR 40-year reanalysis project," *Bulletin of the American Meteorological Society*, vol. 77, no. 3, pp. 437–471, 1996.

[24] H. von Storch, H. Langenberg, and F. Feser, "A spectral nudging technique for dynamical downscaling purposes," *Monthly Weather Review*, vol. 128, no. 10, pp. 3664–3673, 2000.

[25] B. Rockel, A. Will, and A. Hense, "The regional climate model COSMO-CLM (CCLM)," *Meteorologische Zeitschrift*, vol. 17, no. 4, pp. 347–348, 2008.

[26] J. Steppeler, G. Doms, U. Schättler et al., "Meso-gamma scale forecasts using the nonhydrostatic model LM," *Meteorology and Atmospheric Physics*, vol. 82, no. 1–4, pp. 75–96, 2003.

[27] B. Denis, J. Côté, and R. Laprise, "Spectral decomposition of two-dimensional atmospheric fields on limited-area domains using the discrete cosine transform (DCT)," *Monthly Weather Review*, vol. 130, no. 7, pp. 1812–1829, 2002.

[28] X. Xia, M. Zahn, K. Hodges, F. Feser, and H. von Storch, "A comparison of two identification and tracking methods for polar lows," *Tellus A*, vol. 64, Article ID 17196, 2012.

[29] A. Kulkarni and H. von Storch, "Monte Carlo experiments on the effect of serial correlation on the Mann-Kendall test of trend," *Meteorologische Zeitschrift*, vol. 4, no. 2, pp. 82–85, 1995.

[30] H. von Storch and F. W. Zwiers, *Statistical Analysis in Climate Research*, Cambridge University Press, Cambridge, UK, 1999.

[31] U. Luksch, H. von Storch, and E. Maier-Reimer, "Modeling North Pacific SST anomalies as a response to anomalous atmospheric forcing," *Journal of Marine Systems*, vol. 1, no. 1-2, pp. 155–168, 1990.

[32] U. Luksch and H. von Storch, "Modeling the low-frequency sea surface temperature variability in the North Pacific," *Journal of Climate*, vol. 5, no. 9, pp. 893–906, 1992.

[33] J. Bjerknes, "Atlantic air-Sea interaction," *Advances in Geophysics C*, vol. 10, pp. 1–82, 1964.

[34] S. R. Hare and R. C. Francis, "Climate change and salmon production in the Northeast Pacific Ocean," *Canadian Special Publication of Fisheries and Aquatic Sciences*, vol. 121, pp. 357–372, 1995.

[35] Y. Zhang, J. M. Wallace, and D. S. Battisti, "ENSO-like interdecadal variability: 1900–93," *Journal of Climate*, vol. 10, no. 5, pp. 1004–1020, 1997.

[36] N. Mantua, "Comparison of typical warm PDO/El Nino SST, SLP, and wind anomalies," 2000, http://jisao.washington.edu/pdo/graphics.html.

[37] J. M. Wallace and D. S. Gutzler, "Teleconnections in the geopotential height field during the Northern Hemisphere winter," *Monthly Weather Review*, vol. 109, no. 4, pp. 784–812, 1981.